Appl Phys B (2011) 104:897–908
DOI 10.1007/s00340-011-4437-z

Applied Physics B
Lasers and Optics

Cavity-enhanced optical frequency doubler based on transmission-mode Hänsch–Couillaud locking

M. Vainio · J.E. Bernard · L. Marmet

Received: 10 November 2010 / Revised version: 18 December 2010 / Published online: 26 February 2011

Abstract A variant of the Hänsch–Couillaud technique for locking the pump laser frequency to a cavity-enhanced optical frequency doubler is presented. In contrast to the original scheme in which the pump laser light reflected by the enhancement cavity is monitored, the error signal for locking is obtained by polarization analysis of the light transmitted by the cavity. The cavity serves as a spectral and spatial filter for the pump beam, making the transmission-mode locking method particularly useful if the beam quality is poor. Experimental validation of the method is demonstrated by generating more than 190 mW of stable 461 nm light from a cavity-enhanced frequency doubler that is pumped by a diode laser system.

1 Introduction

Optical frequency doubling in a nonlinear crystal, also referred to as second harmonic generation (SHG), is a common method to convert laser light to wavelengths that cannot be directly accessed with lasers. In particular, frequency doubling is often used to generate ultraviolet or blue light. High frequency-doubled power, continuous-wave (cw) operation, and tunable wavelength are required in several applications in laser spectroscopy and atomic physics. As an example, cw 461-nm laser light sources with single-mode operation, good stability, and >100 mW power are needed for laser cooling and trapping of Sr atoms [1–3]. Similar sources for other wavelengths at blue and ultraviolet are needed for experiments with other atomic species [4, 5].

Various implementations of frequency-doubled laser systems for atomic physics have been reported [1–5]. As the efficiency of the doubling process increases with the laser power in the crystal, an external optical build-up cavity is often used to enhance the pump power at the fundamental frequency. The build-up cavity can be either a standing-wave cavity [3] or a traveling-wave ring cavity [6]. For stable continuous-wave operation of the frequency doubler, the frequency of the pump laser needs to be locked to the build-up cavity or vice versa. Usually, locking is done electronically to the center of a cavity resonance peak and a dispersion-like error signal is needed as an input for the lock servo. The most commonly used schemes for generating the error signal are wavelength-modulation spectroscopy [7], Pound–Drever–Hall locking [8], and Hänsch–Couillaud locking [9]. The Hänsch–Couillaud (HC) technique is a form of polarization spectroscopy which differs from most other locking methods in that no modulation of the laser frequency (or power) is needed. The error signal for frequency locking is obtained by monitoring the change in laser light polarization ellipticity due to the build-up cavity. Polarization ellipticity can be made dependent on the cavity frequency detuning by inducing polarization dependent optical loss or birefringence inside the cavity. In the case of a cavity-enhanced frequency doubler, both polarization dependent loss and birefringence contribute to the error signal, owing to the polar-

M. Vainio (✉) · J.E. Bernard · L. Marmet
Institute for National Measurement Standards, National Research Council of Canada, Ottawa, ON, K1A 0R6, Canada
e-mail: markku.vainio@mikes.fi

Present address:
M. Vainio
Centre for Metrology and Accreditation, P.O. Box 9, 02151 Espoo, Finland

Present address:
M. Vainio
Laboratory of Physical Chemistry, Department of Chemistry, University of Helsinki, P.O. Box 55, A.I. Virtasen aukio 1, 00014 Helsinki, Finland

ization dependence of the crystal's nonlinear coefficient and refractive index, respectively.

Extraction of the error signal for frequency locking in the HC method is traditionally done by analyzing the polarization state of the light beam that is reflected by the cavity [9, 10]. In this paper, we discuss an alternative method, in which error-signal detection is done using light transmitted by the cavity [11, 12]. We report on the use of this method to generate >190 mW of stable cw power at 461 nm from a cavity-enhanced optical frequency doubler. The frequency doubler is based on a periodically-poled potassium titanyl phosphate (PPKTP) crystal, which is placed inside a bow-tie ring cavity and pumped by a wavelength tunable master–oscillator–power–amplifier (MOPA) at 922 nm.

The paper is organized as follows. Theoretical study and comparison of the reflection- and transmission-mode HC locking techniques in the context of cavity-enhanced frequency doubling is given in Sect. 2. The experimental setup is described in Sect. 3, and the characteristics of the frequency doubler are reported in Sect. 4. Conclusions are given in Sect. 5.

2 Theory

A typical cavity-enhanced frequency doubler based on a bow-tie ring cavity is schematically shown in Fig. 1. The nonlinear crystal used for frequency doubling is placed between the two curved mirrors, in the primary focus of the cavity. A secondary focus is formed between the plane mirrors. The cavity is made resonant for the fundamental frequency ω in order to enhance the corresponding optical power in the crystal, so as to provide high output power at the doubled frequency 2ω. The frequency doubled power is $P_{\mathrm{shg}} = \Gamma_{\mathrm{shg}} P^2$, where Γ_{shg} is the single-pass conversion efficiency [1/W] and P is the fundamental power in the crystal. The generated power P_{shg} is coupled out of the cavity through a mirror that is highly transmitting at 2ω.

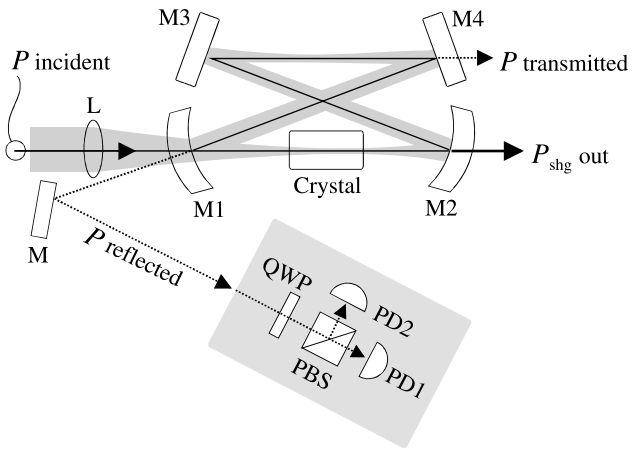

Fig. 1 Schematic of a cavity-enhanced optical frequency doubler. Most of the pump power P incident on the input mirror is mode-matched into the cavity and focused into the nonlinear crystal. Part of the pump power is reflected from the input mirror and a small fraction of the pump power resonating in the cavity leaks out through the mirrors. The generated frequency-doubled power P_{shg} is coupled out of the cavity. The polarization analyzer for generating the error signal in HC locking is depicted *in the gray box*, and discussed later in the text. Abbreviations: M—mirror, PBS—polarizing beam splitter, PD—photodetector, and QWP—quarter wave plate

Efficient coupling and build up of the fundamental field in the cavity is ensured by proper impedance and mode matching. Impedance matching is obtained by using an input coupler mirror whose transmission at ω is such that it exactly compensates for the cavity losses [13]. Mode matching is done by focusing the pump beam into the cavity so that the waist size and position of the focused beam match with the resonating TEM_{00} mode of the cavity. The effect of astigmatism on mode matching, owing to the off-axis focusing by the curved cavity mirrors, can usually be ignored if the folding angle of the cavity is smaller than $\sim 10^\circ$. Equations that describe the fundamental field built up in the cavity can be derived in a standard manner [14]. In the following, we recall the derivation for the case in which the incident pump beam is focused directly into the crystal, between the two curved cavity mirrors. It is straightforward to modify the equations for the case in which mode matching is done to the secondary focus of the cavity instead.

We denote the total pump power mode matched to the TEM_{00} mode of the cavity by P_{in}, and the corresponding electric field by E_{in}. As the HC locking technique relies on polarization spectroscopy, the input power is written as a sum of two orthogonally polarized components $P_{\mathrm{in}} = P_{\mathrm{in},o} + P_{\mathrm{in},e}$, where subscripts o and e refer to ordinarily and extraordinarily polarized light, respectively. The extraordinary polarization is, in this case, the polarization state that provides the highest frequency doubling efficiency. It is normal to the plane of incidence in Fig. 1. The ordinary polarization lies in the plane of incidence and has a negligible frequency doubling efficiency in PPKTP. The fraction of the total mode-matched input power coupled in each polarization is

$$q_x = \frac{P_{\mathrm{in},x}}{P_{\mathrm{in}}}, \tag{1}$$

where the subscript x is either o or e. This notation $x = o, e$ will be used throughout the paper to indicate polarization dependent parameters.

The pump field transmitted by the input mirror M1 of the cavity is

$$E_{\mathrm{M1}(0),x} = (T_{1,x})^{1/2} E_{\mathrm{in},x}, \tag{2}$$

where $T_{1,x}$ is the power transmission of the mirror. We assume a lossless mirror, i.e., $T_{1,x} + R_{1,x} = 1$ if the mirror re-

flectivity is $R_{1,x}$. After $N+1$ number of cavity round trips, the field at mirror M1 becomes

$$E_{\mathrm{M1}(N+1),x} = E_{\mathrm{M1}(N),x}\sqrt{R_{1,x}(1-\gamma_x)}\cdot\exp(i\varphi_x), \tag{3}$$

where $\gamma_x = 1 - R_x^3(1-l)(1-\Gamma P_{\mathrm{cav},x})$ is the round-trip loss excluding the transmission loss $T_{1,x}$ of the input coupler. Here R_x is the average reflectivity of mirrors M2–M4 at the resonating wavelength, and l is the distributed passive fractional loss per round-trip not including the mirror transmission losses. Nonlinear loss due to the crystal, $\Gamma P_{\mathrm{cav},x} = (\Gamma_{\mathrm{shg}} + \Gamma_{\mathrm{abs}})P_{\mathrm{cav},x}$, consists of single-pass frequency doubling efficiency Γ_{shg} and nonlinear absorption loss Γ_{abs} [1], and depends on the fundamental power $P_{\mathrm{cav},x}$ in the crystal. It is important to note that power build-up, and hence also the nonlinear loss is a function of cavity detuning $\exp(i\varphi_x)$. However, for simplicity, we omit this dependence here and assume a constant nonlinear loss that corresponds to the maximum power obtained at a cavity resonance. This approximation is justified because we are mainly interested in what happens close to the center of a resonance peak, which is the lock point of the laser frequency. Moreover, as will be seen in Sect. 4, the error resulting from this approximation is small. Another approximation that can be made if PPKTP is used for frequency doubling is that the nonlinear loss is negligible for the o-polarized wave, i.e., that $\Gamma_o \approx 0$.

The phase term of the field in (3) is given as

$$\varphi_x = 2\pi L_{\mathrm{cav},x}/\lambda + \varphi_{G,x} \tag{4}$$

and it includes the ratio of the optical length $L_{\mathrm{cav},x}$ of the cavity to pump wavelength λ. The additional term $\varphi_{G,x}$ is the Gouy phase shift accumulated over a cavity round-trip. It can be expressed in terms of the cavity ABCD matrix $\mathbf{M}$ [15]

$$\varphi_{G,x} = (1+m+n)\cdot 2\arccos\left[(\mathbf{M}_{0,0}\cdot\mathbf{M}_{1,1})^{1/2}\right], \tag{5}$$

with m and n referring to transverse (Hermite–Gaussian) mode numbers of the resonating field. The subscripts of $\mathbf{M}$ denote the matrix elements. Because of the birefringence of the nonlinear crystal and cavity mirrors, the Gouy phase shift is, in general, different for different polarizations.

By combining (2) and (3), the total field built up at the input mirror M1 can be written as

$$\begin{aligned} E_{\mathrm{M1},x} &= \sqrt{T_{1,x}}E_{\mathrm{in},x}\sum_{N=0}^{\infty}\left[\sqrt{R_{1,x}(1-\gamma_x)}\cdot\exp(i\varphi_x)\right]^N \\ &= \frac{\sqrt{T_{1,x}}}{1-\sqrt{R_{1,x}(1-\gamma_x)}\cdot\exp(i\varphi_x)}E_{\mathrm{in},x}, \end{aligned} \tag{6}$$

and the corresponding optical power in the cavity as

$$\begin{aligned} P_{\mathrm{cav},x} &= \left(\frac{E_{\mathrm{M1},x}}{E_{\mathrm{in},x}}\right)^2 P_{\mathrm{in},x} \\ &= T_{1,x}\left[1-\sqrt{R_{1,x}(1-\gamma_x)}\cdot\exp(i\varphi_x)\right]^{-2}P_{\mathrm{in},x}. \end{aligned} \tag{7}$$

The cavity build-up factor, i.e., the factor by which the mode-matched fundamental power is enhanced by the cavity at resonance (φ_x being a multiple of 2π), is

$$BUF_x = \frac{P_{\mathrm{cav},x}}{P_{\mathrm{in},x}} = \left(\frac{\sqrt{T_{1,x}}}{1-\sqrt{R_{1,x}(1-\gamma_x)}}\right)^2. \tag{8}$$

The build-up factor is related to the optical finesse F of the (ring) cavity through $BUF = F/\pi$.

2.1 Reflection-mode HC locking

In its most common implementation, the error signal for HC locking is extracted by monitoring the polarization ellipticity of the light reflected from the cavity input mirror [9]. The incoming light is linearly polarized and can be presented as a superposition of two orthogonal polarization components, e.g., the e- and o-polarized waves. A half-wave plate before the cavity can be used to adjust the fraction of light, q_x, in each polarization. The reflected field $E_{R,x}$ can be expressed as a superposition of direct reflection from the mirror (M1, Fig. 1) and the field leaking out of the cavity through the mirror:

$$\begin{aligned} E_{R,x}(\Delta L_{\mathrm{cav}}) = \sqrt{R_{1,x}}e^{i\pi}E_{\mathrm{in},x} + \sqrt{T_{1,x}(1-\gamma_x)} \\ \times\exp\left[i\varphi_x + 2\pi i(\Delta L_{\mathrm{cav}}/\lambda)\right]\cdot E_{\mathrm{M1},x}. \end{aligned} \tag{9}$$

Respectively, the power reflected by the cavity for each polarization is

$$\begin{aligned} P_{R,x}(\Delta L_{\mathrm{cav}}) &= \left(\frac{E_{R,x}(\Delta L_{\mathrm{cav}})}{E_{\mathrm{in},x}}\right)^2 P_{\mathrm{in},x} \\ &= \left(\frac{E_{R,x}(\Delta L_{\mathrm{cav}})}{E_{\mathrm{in},x}}\right)^2 q_x P_{\mathrm{in}}. \end{aligned} \tag{10}$$

Note that field $E_{\mathrm{M1},x}$ built up in the cavity is defined as the field at the surface of mirror M1, just *after* it has been reflected by the mirror. Therefore, the field has to be circulated in the cavity once more before it can be coupled out through the mirror. This is included in (9) by multiplying $E_{\mathrm{M1},x}$ by the (complex) round-trip transmission of the cavity. In order to account for frequency detuning between the pump laser and the build-up cavity, we have now written the reflected field as a function of cavity length detuning ΔL_{cav}. (The fractional frequency tuning is equal to the fractional change of the cavity length.)

The original demonstration of the HC-technique was done using a polarizer inside the cavity in order to produce high loss for one of the polarization components while allowing the other one to resonate with low loss [9]. Ideally, the first polarization component would experience such a high intracavity loss that it would be entirely reflected by the input mirror, thus providing a constant phase reference

for error signal measurement. When a wave circulating in the cavity is exactly in resonance, it remains in phase with the incident field, and the total reflected field that includes a component leaking out of the cavity remains linearly polarized. If the circulating field is out of resonance, the phase either lags or leads relative to the incident field, depending on the sign of the detuning. Consequently, the total light reflected by the cavity becomes elliptically polarized. The sign of the laser frequency detuning from the nearest cavity resonance can then be determined based on the handedness of this polarization ellipticity. The ellipticity is typically measured using a polarization analyser composed of a quarter wave plate, a polarizing beam splitter, and two photodiodes that monitor the powers transmitted to the two output arms, A and B, of the beam splitter [9]. The analyzer is schematically depicted in Fig. 1. The signals detected by the photodiodes can be calculated using Jones calculus. The Jones matrix for a quarter wave plate that has the fast axis horizontally aligned is

$$\mathbf{M}_{\mathrm{QWP}} = \begin{bmatrix} 1 & 0 \\ 0 & e^{-i\pi/2} \end{bmatrix}. \tag{11}$$

Rotation of the wave plate by angle θ is given by the transformation

$$\mathbf{HC}(\theta) = \mathbf{R}(-\theta)\mathbf{M}_{\mathrm{QWP}}\mathbf{R}(\theta), \tag{12}$$

where

$$\mathbf{R}(\theta) = \begin{bmatrix} \cos(\theta) & \sin(\theta) \\ -\sin(\theta) & \cos(\theta) \end{bmatrix}. \tag{13}$$

With the help of (9) and (12), the electric fields detected by the photodiodes A and B, respectively, can be expressed as [9]

$$\begin{aligned} E_{\mathrm{PD\_A}}(\Delta L_{\mathrm{cav}}) &= \mathbf{HC}_{0,0}(\theta)E_{R,o}(\Delta L_{\mathrm{cav}}) \\ &\quad -\mathbf{HC}_{0,1}(\theta)E_{R,e}(\Delta L_{\mathrm{cav}}), \end{aligned} \tag{14a}$$

$$\begin{aligned} E_{\mathrm{PD\_B}}(\Delta L_{\mathrm{cav}}) &= \mathbf{HC}_{1,0}(\theta)E_{R,o}(\Delta L_{\mathrm{cav}}) \\ &\quad -\mathbf{HC}_{1,1}(\theta)E_{R,e}(\Delta L_{\mathrm{cav}}), \end{aligned} \tag{14b}$$

where the subscripts of **HC** refer to the matrix elements.

The corresponding optical powers are

$$\begin{aligned} P_{\mathrm{PD\_A}}(\Delta L_{\mathrm{cav}}) &= \big[q_o\mathbf{HC}_{0,0}(\theta)E_{R,o}(\Delta L_{\mathrm{cav}}) \\ &\quad - q_e\mathbf{HC}_{0,1}(\theta)E_{R,e}(\Delta L_{\mathrm{cav}})\big]^2 P_{\mathrm{in}}, \end{aligned} \tag{15a}$$

$$\begin{aligned} P_{\mathrm{PD\_B}}(\Delta L_{\mathrm{cav}}) &= \big[q_o\mathbf{HC}_{1,0}(\theta)E_{R,o}(\Delta L_{\mathrm{cav}}) \\ &\quad - q_e\mathbf{HC}_{1,1}(\theta)E_{R,e}(\Delta L_{\mathrm{cav}})\big]^2 P_{\mathrm{in}}. \end{aligned} \tag{15b}$$

The HC error signal ΔU_{HC} is usually a voltage signal and it is proportional to the difference of the two photodiode signals,

$$\Delta U_{\mathrm{HC}}(\Delta L_{\mathrm{cav}}) = G\big[P_{\mathrm{PD\_A}}(\Delta L_{\mathrm{cav}}) - P_{\mathrm{PD\_B}}(\Delta L_{\mathrm{cav}})\big], \tag{16}$$

with G[V/W] being the power-to-voltage conversion factor, which includes the gains of the photodiode amplifiers etc.

If the e-polarized wave is the one used for frequency doubling, the o-polarization serves as the phase reference for the error signal measurement. In contrast to the original concept of HC locking, the reference polarization (o) is the one that experiences lower losses. This is because the frequency doubling process produces an additional loss for the e-polarized field. Such nonlinear loss can be significantly higher than the linear (passive) loss of the build-up cavity. Nevertheless, a dispersion-like error signal is obtained as long as the two polarizations experience different losses. This is demonstrated in Fig. 2a, which shows a simulation of the HC error signal as calculated using (16) for a typical cavity-enhanced frequency doubler. The parameters were chosen to match those of our experimental setup, which is described in Sects. 3 and 4. The total round-trip losses of $\gamma_o \approx 0.02$ and $\gamma_e \approx 0.095$ were assumed for the o- and e-polarized wave, respectively. The strongest error signal would be obtained by dividing the input power equally between the o- and e-polarized waves. The 50/50 splitting ratio is, however, not practical with the frequency doubler—we want to maximize the frequency doubling efficiency by coupling as much power as possible into the e-polarized wave. The simulations have been done with $q_o = 0.01$ of the total input power coupled into the reference (o) polarization, which is the same fraction as typically used in our experiments.

The simulation of Fig. 2a is based on the assumption that both polarization components share the same phase velocity and thus have exactly the same resonance frequencies. In practice, the cavity mirrors and especially the nonlinear crystal are birefringent, and the resonance frequencies of the o-polarized wave are shifted from those of the e-polarized wave. This birefringence alone is sufficient to produce an error signal because the o-polarized wave is out of resonance and serves as a reference whenever the e-polarized wave is in resonance. An example of an error signal generated by a birefringent cavity is shown in Fig. 2b. The simulation was done assuming equal losses of $\gamma_e = \gamma_o \approx 0.02$ for both polarization components, and by including an arbitrarily chosen phase term $\Delta\varphi_{\mathrm{br}} = -0.75\pi$ to describe the birefringence ($\varphi_o = \varphi_e + \Delta\varphi_{\mathrm{br}}$). Other parameters are the same as in Fig. 2a.

The case of Fig. 2b in which the HC error signal arises from crystal birefringence only has previously been discussed in reference [16]. However, the discussion is valid

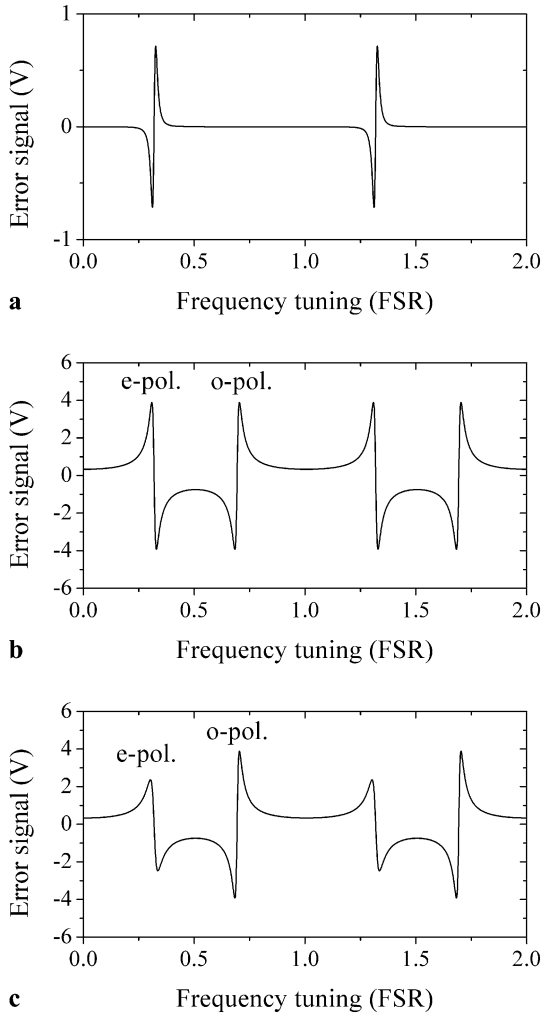

Fig. 2 Simulations of HC error signals in the reflection-mode scheme as a function of cavity frequency tuning relative to the pump laser frequency. The spectra are repeated after every FSR (free spectral range) of the cavity. Frequency scan over 2 FSRs is shown. The error signal is generated as a result of (**a**) polarization dependent loss in the cavity/crystal without birefringence, in which case the resonance frequencies of the *o*- and *e*-polarized waves are the same; (**b**) cavity/crystal birefringence; and (**c**) both birefringence and polarization dependent loss. All simulations have been done with $\theta = 45°$

only if the two polarizations, extraordinary and ordinary, experience the same intracavity loss. With most cavity-enhanced frequency doublers the nonlinear loss process is significant and cannot be neglected. Consequently, the error signal is produced as a combination of the two effects: birefringence and polarization dependent intracavity loss. A simulation of the error signal in this case is plotted in Fig. 2c using the same parameter values as in Figs. 2a and 2b.

The simulated error signals shown above are very smooth and distinct, which is not always true for real signals. A common reason for error signal degradation is a non-Gaussian profile of the pump beam. This is particularly true for the systems based on high-power semiconductor tapered amplifiers discussed in this paper. Spatial quality of the output beam of a tapered amplifier is typically rather poor, allowing a TEM_{00} mode-matching efficiency of only about 60–80%. This means that a substantial amount of the input power is reflected by the build-up cavity even at the center of cavity resonance, which degrades the contrast of the reflection fringes. Most of the reflected power is in higher order transverse modes, and these modes cause additional features and ripple in the error signal spectrum. This is a problem especially if the resonance peaks of higher order transverse modes partially overlap with the fundamental mode used for laser locking. Quantitative prediction of the error signal is further complicated by different Gouy phase shifts experienced by different transverse modes as they travel from the cavity input mirror to the polarization analyzer. As the polarization analyzer measures the phase difference between the *o*- and *e*-polarized waves—which can be different for different transverse modes—the variations of the amplifier's output beam profile are potentially converted into variations of the lock-point offset. The beam profile of a tapered amplifier depends, e.g., on the injection current [1]. Poor quality and changes of the beam profile can be problematic in systems that require good long-term stability. These include, for instance, magneto–optical traps used in optical atomic clocks.

2.2 Transmission-mode HC locking

The quality of the pump beam can be improved by spatial filtering, for example, by coupling the laser beam through a single-mode optical fiber. However, adding an extra filter increases the system complexity and inevitably leads to a reduction of the TEM_{00} power. These problems can be avoided by using an error signal detection scheme based on cavity transmission rather than reflection. The build-up cavity itself works as a spatial and spectral filter for the input beam, providing a clean error signal even if the input beam quality is poor. The cavity also filters out most of the amplified spontaneous emission, which can be up to several percent of the total output power of a tapered amplifier. Altogether, as the quality of the transmitted beam does not significantly depend on the quality of the input beam, the effect of imperfect mode-matching can be easily taken into account when simulating the error signal.

The error signal detector assembly used for transmission-mode Hänsch–Couillaud (TMHC) locking is identical to that used in the conventional reflection-mode locking scheme. The only difference is that the polarization analyzer is now placed behind a cavity mirror so that it detects light transmitted by the cavity. As an example, for the cavity geometry of Fig. 1, the field built up at the input mirror of the build-up cavity has to travel through the crystal and be

reflected by mirrors M2 and M3 before it is partially transmitted by mirror M4 for error signal detection. The field transmitted by mirror M4 is written

$$E_{T,x}(\Delta L_{\mathrm{cav}}) = \sqrt{R_x^2(1-l)(1-\Gamma P_{\mathrm{cav},x})}\sqrt{T_{4,x}} \times \exp\left[i\varphi_{\mathrm{OC},x} + 2\pi i(\Delta L_{\mathrm{cav}}/\lambda)\right] E_{\mathrm{M1},x}, \quad (17)$$

and the corresponding optical power is

$$P_{T,x}(\Delta L_{\mathrm{cav}}) = \left(\frac{E_{T,x}(\Delta L_{\mathrm{cav}})}{E_{\mathrm{in},x}}\right)^2 P_{\mathrm{in},x} = \left(\frac{E_{T,x}(\Delta L_{\mathrm{cav}})}{E_{\mathrm{in},x}}\right)^2 q_x P_{\mathrm{in}}. \quad (18)$$

In (17), the transmission of the mirror used for signal output coupling is denoted by $T_{4,x}$. The phase shift $\varphi_{\mathrm{OC},x} = 2\pi L_{\mathrm{OC},x}/\lambda + \varphi_{\mathrm{OC\_}G,x}$ accounts for the optical path length $L_{\mathrm{OC,x}}$ between mirror M1 and the TMHC detector assembly and $\varphi_{\mathrm{OC\_}G,x}$ is the respective Gouy phase shift. In addition, when using the TMHC signal output coupling geometry shown in Fig. 1, the phase of the field traveling from M1 to the TMHC detector assembly depends on cavity length tuning ΔL_{cav}. This is denoted by the second phase term in (17). Other parameters used in (17) have been defined previously, and the field $E_{\mathrm{M1},x}$ built up at the input coupler is given by (6). Note that if the average mirror transmission losses $T_x = 1 - R_x$ are negligible compared to other intracavity losses, (17) can be simplified by approximating $R_x^2(1-l)(1-\Gamma P_{\mathrm{cav},x}) \approx 1-\gamma_x$ because the round-trip loss is $\gamma_x = 1 - R_x^3(1-l)(1-\Gamma P_{\mathrm{cav},x})$, see (3).

By inserting the transmitted fields $E_{T,x}(\Delta L_{\mathrm{cav}})$ given by (17) into (15) instead of $E_{R,x}(\Delta L_{\mathrm{cav}})$, the generated TMHC error signal can now be calculated from (16) exactly the same way as before in the case of reflection-mode locking. The imperfect TEM_{00} mode-matching efficiency is taken into account by introducing a mode-matching coefficient κ_x, which allows us to write the mode-matched power as $P_{\mathrm{in},x} = \kappa_x P_{\mathrm{inc},x}$ where $P_{\mathrm{inc},x}$ is the total incident pump power in the given polarization. (Respectively $E_{\mathrm{in},x} = \sqrt{\kappa_x} E_{\mathrm{inc},x}$). In practice, the mode matching coefficient can be determined by measuring the fringe contrast of the reflection spectrum of an impedance matched cavity.

Equations similar to (17) and (18) can be written for the transmitted TEM_{01} modes as well, taking into account different Gouy phase shifts (5). Since the TEM_{01} mode has two lobes with opposite polarizations, it does not produce an interference signal with the TEM_{00} mode if the entire beam is sampled by the photodetector. Moreover, if the mode-matching is done properly, transverse modes of higher order than TEM_{01} have only a negligible contribution to the total transmitted field. This allows us to write the total transmitted power as a sum of powers in the TEM_{00} and TEM_{01} modes. Likewise, the TMHC error signal, given by (16), is obtained as a sum of error signals calculated separately for each transverse mode.

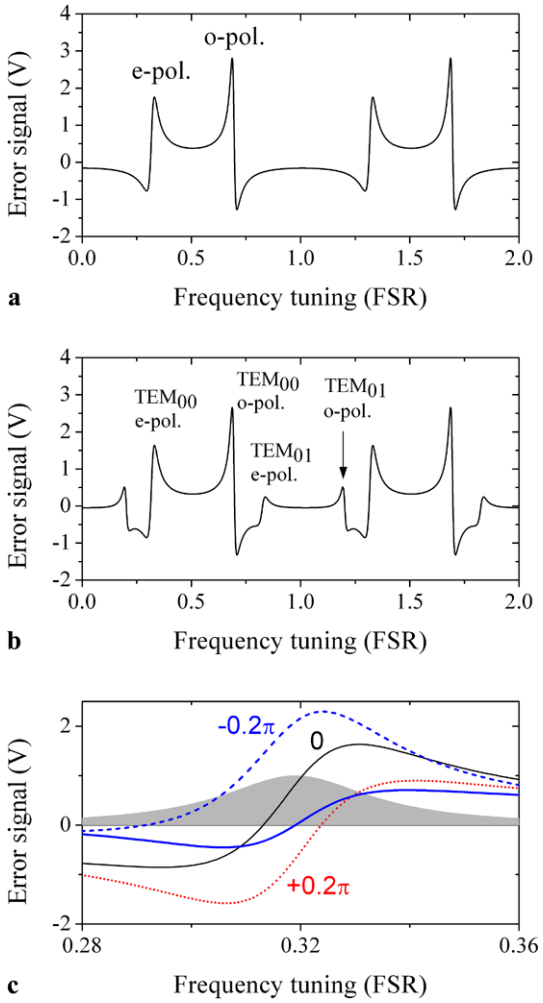

Fig. 3 Simulations of TMHC error signals in the transmission-mode scheme as a function of cavity frequency tuning relative to the pump laser frequency. (**a**) Error signal calculated for conditions similar to those used for the simulation of Fig. 2c. (**b**) The same but with some of the pump power coupled into the TEM_{01} modes of the cavity. (**c**) A close-up of the error signal generated around the *e*-polarized TEM_{00} resonance peak. *The filled gray curve* shows the cavity resonance peak for reference. Simulations with three different values of $\Delta\varphi_{\mathrm{OC}}$ (-0.2π, 0, and $+0.2\pi$) are shown, see text for details. The curve with $\Delta\varphi_{\mathrm{OC}} = 0$ is the same as the one plotted in (**b**). The unlabeled *solid curve* has been calculated for $\Delta\varphi_{\mathrm{OC}} = -0.2\pi$ but with $\theta = 48°$ and with an offset of +0.2 V, which gives an error signal that has a zero-crossing at the center of the resonance peak. All other simulations with $\theta = 45°$ and without an offset

Figure 3a shows the simulated error signal for a built-up cavity that has both birefringence and polarization dependent losses, i.e., for conditions similar to those used to calculate the signal of Fig. 2c. In Fig. 3b, we have repeated the same calculation for a more realistic case in which the

TEM_{00} coupling efficiency is smaller than 100% and some light is coupled in the TEM_{01} modes as well. We have assumed similar mode-matching efficiencies for the o- and e-polarized waves, $\kappa_{oe} = 0.7$ for TEM_{00} and $\kappa_{oe} = 0.2$ for TEM_{01} modes, respectively. These values were chosen to match our experimental values, although in practice the two polarizations often have different mode-matching efficiencies, as will be discussed in Sect. 4. Also, the optical powers ($P_{\mathrm{inc},e} = 430$ mW and $P_{\mathrm{inc},o} = 4$ mW) incident on the input mirror M1 are typical to our experimental setup. Cavity losses ($\gamma_e \approx 0.095$ and $\gamma_o \approx 0.02$) were assumed to be the same for both TEM_{00} and TEM_{01} modes. Gouy phase shifts that determine the transverse mode separation were calculated from (5) for a cavity similar to the one used in our experiments and described in more detail in Sect. 3.

Although the general appearance of the transmission-mode HC locking error signal is similar to that of reflection-mode locking, its physical origin is somewhat different. In the reflection mode, the imaginary part of the reflection coefficient of the e-polarized wave is measured using the o-polarized wave as a reference (or vice versa). In the case of a cavity-enhanced frequency doubler, some of the o-polarized light is coupled into the cavity but the reference field is still dominated by the fraction of the field that is directly reflected by the input coupling mirror. This provides a constant phase reference that is independent of the laser frequency tuning. The case of mode degeneracy exemplified in Fig. 2a is an exception. Transmission-mode locking, on the other hand, relies on the use of the transmitted o-polarized field as a reference. This means that the phase of the reference field varies as a function of cavity detuning.

As is evident from (17), the error signal depends also on the phase difference $\Delta\varphi_{\mathrm{OC}} = \varphi_{\mathrm{OC},o} - \varphi_{\mathrm{OC},e}$ accumulated as the waves travel from the input mirror M1 to the HC detector assembly. This is demonstrated in Fig. 3c, which shows simulations of the error signal of the e-polarized TEM_{00} peak with three different values of $\Delta\varphi_{\mathrm{OC}}$. It is worth noting that the absolute value of $\varphi_{\mathrm{OC},x}$ does not matter, just the changes in the phase difference $\Delta\varphi_{\mathrm{OC}}$. The additional phase difference makes quantitative prediction of the error signal shape difficult, as the phase difference depends on things like crystal temperature and cavity alignment. A similar effect on the error signal would be caused, e.g., by polarization ellipticity of the input beam or by imperfections of the wave plate or polarizing beam splitter of the detector assembly. In any case, the error signal shape and zero-crossing point can be empirically optimized for any value of $\Delta\varphi_{\mathrm{OC}}$ by rotating the quarter wave plate of the detector assembly, and by applying an offset to the error signal. This is demonstrated in Fig. 3c.

3 Experimental setup

We have used the transmission-mode HC locking scheme to generate more than 190 mW of blue light at 461 nm from a cavity-enhanced frequency doubler, which is outlined in Fig. 4. The doubler is pumped by a MOPA, which consists of two parts: A home-built external-cavity diode laser (ECDL) that is based on the design reported by Hawthorn et al. [17], and a commercial tapered amplifier (Toptica BoosTA). The ECDL has a coarse tuning range from 914 to 985 nm, and a mode-hop-free fine tuning range of 3–6 GHz, depending on the operating wavelength. We usually operate the ECDL at 922 nm, where it emits more than 15 mW of output power. The ECDL output beam is passed through a −60 dB optical isolator and circularized using an anamorphic prism pair before mode-matching it into the tapered amplifier. The maximum output power of the amplifier is 500 mW. The

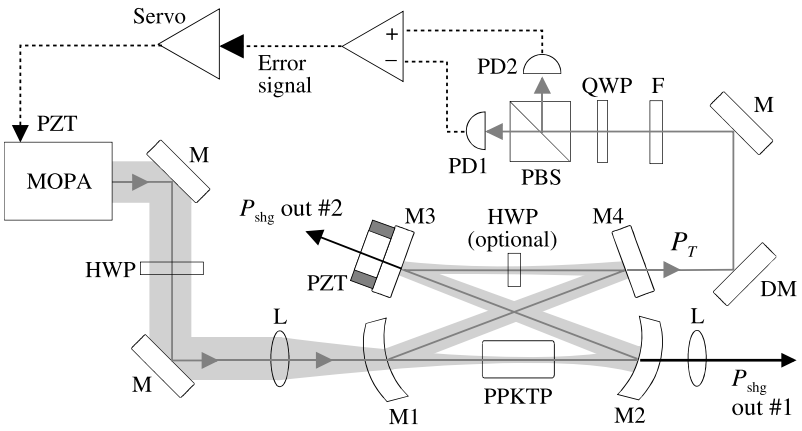

Fig. 4 Illustration of the experimental setup. Optical signals/beams are indicated by *solid lines* and electronic signals are shown by *dashed lines*. Abbreviations: DM—dichroic mirror that reflects 922 nm and transmits blue, F—long-pass filter, HWP—half wave plate, L—lens, M—mirror, PBS—polarizing beam splitter cube, PD1 and PD2—photodetectors, QWP—quarter wave plate. Other symbols and abbreviations are explained in the text

output beam of the amplifier is circularized using another anamorphic prism pair, passed through a −30 dB optical isolator, and mode-matched into the build-up cavity used for frequency doubling. At the maximum power of the MOPA, we get up to 430 mW of 922-nm laser light incident on the cavity. A half-wave plate before the cavity is used to adjust the light polarization state. A small fraction, ∼1% of the total power, is coupled to the *o*-polarized reference wave while the rest is used for efficient frequency doubling in *e*-polarization.

The build-up cavity is a standard bow-tie cavity, which consists of two plane mirrors and two concave mirrors that have a radius of curvature of 75 mm each. The geometric separation between the concave mirrors is 96 mm, and the distance from a concave mirror to the secondary focus of the cavity is 155 mm. The folding angle of the cavity is ∼10°, which leads to a calculated astigmatism of smaller than 4%, defined as $(w_{\mathrm{sag}} - w_{\mathrm{tan}})/w_{\mathrm{sag}}$, where w_{sag} and w_{tan} are the waist sizes of the resonating beam in the sagittal and tangential planes, respectively. The input coupler (M1) has a reflectivity of approximately 90% at 922 nm, which was chosen so as to optimize the impedance matching of the cavity at the maximum frequency doubled power, taking into account the nonlinear loss owing to the frequency doubling process [1]. All other cavity mirrors have high reflectivity of $R_{oe} \approx 0.999$ at $\lambda = 922$ nm, and transmission of 94% at $\lambda/2 = 461$ nm. The transmission for 461 nm allows us to extract a fair amount of blue light through two separate mirrors. Most (94%) of the generated blue power is coupled out through the second curved mirror M2, leaving approximately 5% of the total power in the secondary output beam that is extracted through mirror M3. This dual-output design is useful in many applications, since the weaker beam can be used for wavelength monitoring or locking, while the high-power output is directed to the actual experiment.

The nonlinear crystal used for frequency doubling is similar to that used in a previous work of Le Targat et al. [1]. It is a 20-mm long PPKTP crystal (Raicol), whose end facets are antireflection coated for both 922 and 461 nm. The poling period of the crystal is 5.5 μm, and the optimum phase matching at 922 nm is obtained at a crystal temperature of approximately 30°C. The crystal is mounted in a copper holder, which is covered by a Teflon cap. The crystal holder is in good thermal contact with the cavity base plate that is made of copper as well. The whole baseplate/crystal holder assembly is temperature stabilized using Peltier elements and a single controller. Temperature stability of better than 10 mK was measured with the temperature sensor used for stabilization. The sensor is attached in close proximity with the crystal. The cavity unit is placed inside of an aluminium box for improved long-term stability of the frequency doubled light.

While most reported cavity-enhanced frequency doublers have the input pump beam mode-matched in the secondary focus of the bow-tie cavity, we have used a design in which the input beam is focused directly into the nonlinear crystal [2]. The advantage of this approach is that it decouples the cavity alignment from the input beam alignment. (The same advantage can also be obtained by coupling the input light directly to the first curved mirror (M1, Fig. 1) through plane mirror M4, in which case the coupling focus lies outside the cavity.) In the more commonly used design, any change of the cavity alignment also changes the alignment of the input beam to the crystal, which is problematic since both phase matching and HC error signal depend on this alignment. By using the scheme of Fig. 4, we can first optimize the phase matching temperature for a given alignment of the input beam. This optimization is most conveniently done in the single-pass frequency doubling configuration, with the cavity resonance blocked. Alignment of the cavity can then be independently optimized without affecting the phase matching condition, making the alignment process simpler and faster than with the other approach. We have used a single plano-convex lens ($f = 100$ mm) to mode match the input beam into the cavity, which is designed to have a waist size of ∼42 μm in the middle of the crystal. This corresponds to a focusing parameter of $\xi = 0.9$ [18], which has been shown to provide a high frequency doubling efficiency in a system similar to ours without suffering from significant thermal effects that could compromise the servo lock stability [1].

The polarization analyzer used for HC error signal detection consists of a rotatable zero-order quarter wave plate, a polarizing beam splitter, and two Si-photodiodes. Large area photodiodes are used in order to ensure that entire beams are sampled. Clipping of the beams could lead to additional features in the error signal spectrum due to transverse-mode interference [19–21]. Furthermore, we carefully designed the analyzer assembly so that no interference is produced on the error signal by room lights or by residual 461 nm light which leaks through the build-up cavity. The analyzer is sealed in a closed unit, which has an optical long pass filter (Thorlabs FEL850) at the input to block out visible light.

It should be noted that no optical attenuation for 922 nm is needed before the polarization analyser. A standard high-reflectivity mirror (M4, $R = 99.9\%$) reduces the optical power incident on the photodiodes to the required milliwatt level. In our experiments, we have used mirrors that are highly reflective for both polarizations. This means that only about 1–100 μW of *o*-polarized power is transmitted through the cavity, depending on the frequency separation of the resonance peaks of the *o*- and *e*-polarized waves. Although this is sufficient to produce a good quality error signal, better signal-to-noise ratio could probably be obtained by using a mirror that has a higher transmission coefficient for the *o*-polarization.

The photocurrent signals of the photodiodes are converted into voltage signals using transimpedance amplifiers

and subsequently fed into a differential amplifier that generates the TMHC error signal; see (15) and (16). The gain of each photodiode channel can be tuned independently, which makes it possible to adjust the error signal, essentially in the same way as by rotating the quarter wave plate of the polarization analyzer. In addition, we have implemented an offset potentiometer that can be used to add a small voltage offset to the error signal for fine adjustment of the lock point. The error signal is fed into servo electronics (PI-controller) whose output is connected to a high-voltage amplifier that controls the ECDL frequency through a piezoelectric actuator (PZT). The ECDL frequency is thus locked to that of the external build-up cavity. Frequency of the blue 461 nm beam can be adjusted and scanned using a PZT that controls the build-up cavity length by actuating mirror M3 (Fig. 4).

A common problem with the Hänsch–Couillaud locking method, both in the reflection- and transmission-mode, is that the error signal depends on several parameters such as crystal temperature, crystal alignment, and build-up cavity alignment. Depending on these and various other system parameters, it may happen that the resonance peaks of the *o*- and *e*-polarized waves overlap so much that the error signal gets distorted at resonance. If the two resonances overlapped exactly, there would be no problem since we would get a signal similar to that of Fig. 2a. However, a small deviation from the degeneracy distorts the signal, making reliable locking to a resonance peak difficult. This can be most easily avoided by adjusting the crystal temperature, which shifts the resonance peaks of different polarizations relative to each other, owing to the temperature dependence of the crystal birefringence. However, this method works poorly with frequency doublers, since the crystal temperature should be optimized for phase matching and is thus not a free parameter. Another way of changing the relative positions of the *o*- and *e*-polarized waves' resonance peaks is to change the cavity alignment. This method is just as problematic, not only because of the resulting changes in phase matching, but also because the alignment affects the power build-up in the cavity. A systematic search of suitable resonance frequencies by varying the cavity alignment is very difficult.

We solved the problem of possibly overlapping resonance frequencies by adding a half-wave plate inside the frequency doubler cavity. It is placed in the secondary focus of the cavity; see Fig. 4. The wave plate is antireflection coated for 922 nm and slightly tilted in order to avoid disturbing the cavity resonance. The wave plate rotation angle is first adjusted for the maximum blue output power. The angle is then slightly rotated around this point in order to alter the cavity birefringence and to find a setting that produces a cavity transmission spectrum with well separated resonance peaks for the two orthogonal polarizations. The intracavity wave plate was not used in the measurements reported in this paper, but we have used it routinely in later experiments. The addition of the wave plate improves the usability of the frequency doubler in the long term, as possible changes in the error signal spectrum caused by thermal drifts, etc. can easily be compensated for by adjusting the wave plate. As a drawback, the wave plate increases cavity losses and reduces the attainable blue output power. A power reduction of about 3–6% was typically observed when having the wave plate rotation angle close to that corresponding to the maximum output power.

4 Results

At the maximum fundamental power of 430 mW incident to the frequency doubler build-up cavity, 68–70% of the power is mode-matched into the TEM_{00} mode of the cavity. This gives an intracavity power of about 3 W and a power enhancement factor of $BUF = P_{\mathrm{cav}}/P_{\mathrm{in}} = 10$ (as defined in (8)). The generated second harmonic power at 461 nm is up to 200 mW, which corresponds to a single-pass efficiency of $\Gamma_{\mathrm{shg}} = 0.022$ 1/W, in agreement with that reported by Le Targat et al. for a similar crystal [1]. Most (170–190 mW) of the blue power is extracted through the second curved mirror (M2, Fig. 4). The secondary output through the flat mirror M3 produces up to ∼10 mW of blue light.

As demonstrated in Fig. 5, thermal effects in the crystal are modest and do not disturb the servo lock. This allows us to reach the same output power both in the cavity-swept (pulsed) mode and locked cw mode. Sometimes, we observe a slow decay of a couple of percent in the cw output power just after locking the ECDL frequency to the build-up cavity. However, the peak power cannot be recovered by

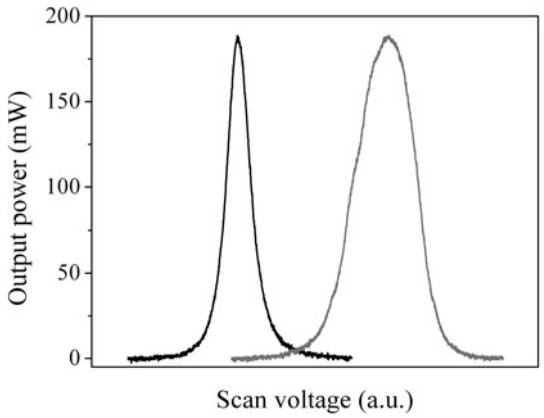

Fig. 5 Blue output power through mirror M2 (see Fig. 4) when slowly scanning the length of the build-up cavity without locking the ECDL to it. *Black curve*: expanding cavity. *Gray curve*: contracting cavity (x-axis offset for clarity). Scan speed is 25 GHz/s (1 FSR in 50 ms). The difference in the fringe widths indicates small thermal effects [1]. The blue output power emitted through the mirror is 186 mW, which corresponds to a generated power of about 195 mW (outside of the crystal)

adjusting the PPKTP temperature, which suggests that the power decay is not caused by a deviation from the optimum phase-matching temperature. Instead, we are able to recover the output power by a small adjustment of the build-up cavity alignment, which suggests that the reason for the power drop is a thermally induced cavity misalignment, owing to either heating of the cavity mirrors or, more likely, heating of the crystal. Although the crystal front facet is antireflection coated for 922 nm, it reflects back some of the resonant pump power and forces the MOPA to optically lock to the build-up cavity if the crystal is perfectly aligned for normal incidence of the pump beam. This optical locking is similar to that reported in [10], and it makes the electronic servo lock unstable. In order to eliminate the optical feedback, the PPKTP was slightly tilted relative to the optical axis. Such a tilt is expected to make the cavity alignment weakly temperature dependent owing to temperature dependence of the crystal refractive index. The need for crystal tilting could probably be avoided by replacing the optical isolator with a double-stage isolator that provides isolation better than 60 dB.

We studied the TMHC error signal by recording it as a function of laser detuning. During the study, the ECDL frequency was kept constant and the build-up cavity frequency was scanned over more than one free spectral range (FSR) by scanning the cavity length. Also, the 922-nm power reflected from the cavity input mirror was recorded vs. cavity scanning. The scan rate was relatively fast (1 FSR in 6 ms) and the temperature of the crystal was not allowed to change significantly. Therefore, the influence of thermal effects on the error signal was negligible. An example of the cavity reflection spectrum is shown in Fig. 6a together with a trace simulated based on the theory (10) presented in Sect. 2.1. The corresponding TMHC error signals, both experimental and theoretical, are shown in Fig. 6b. Figure 6c shows a simulation of the cavity transmission spectrum. This was calculated using (18). The following parameter values were used: $\lambda = 922$ nm, $\theta = 42°$, $P_{\mathrm{inc}} = 430$ mW, $q_o = 0.015$, $\kappa_e = 0.68$ (TEM$_{00}$), $\kappa_e = 0.058$ (TEM$_{01}$), $\kappa_o = 0.38$ (TEM$_{00}$), $\kappa_o = 0.2$ (TEM$_{01}$), $R_e = 0.999$, $R_o = 0.9988$, $R_{\mathrm{M}1e} = 0.902$, $R_{\mathrm{M}1o} = 0.895$, $R_{4e} = R_{4o} = 0.9988$, $\gamma_e = 0.0935$ (TEM$_{00}$), $\gamma_e = 0.16$ (TEM$_{01}$), $\gamma_o = 0.058$ (TEM$_{00}$), $\gamma_o = 0.25$ (TEM$_{01}$), $l = 0.02$, $\Gamma_{\mathrm{shg}} = 0.022$ 1/W, and $\Gamma_{\mathrm{abs}} = 0.006$ 1/W. In addition, we have taken into account the photodiode responsivity (0.7 A/W), the transimpedance amplifier gain (10^4 V/A), and the difference amplifier gain (11.4), giving $G \approx 8 \times 10^4$ V/W for the power-to-voltage conversion factor of (16). The phase terms defined in (4) were determined from the measured longitudinal and transverse mode spacing of the cavity. The cavity birefringence and the phase difference $\Delta\varphi_{\mathrm{OC}}$, which depend on several factors, such as cavity alignment, are tedious if not impossible to measure and were therefore adjusted to give the best fit to the experimentally data. As we have demonstrated in Fig. 3c, changes in $\Delta\varphi_{\mathrm{OC}}$ can significantly alter the error signal spectrum, although the positions of the cavity resonance peaks remain unchanged. After finding the appropriate phase terms, very good agreement was obtained between the experimental and simulated error signals. The resonance

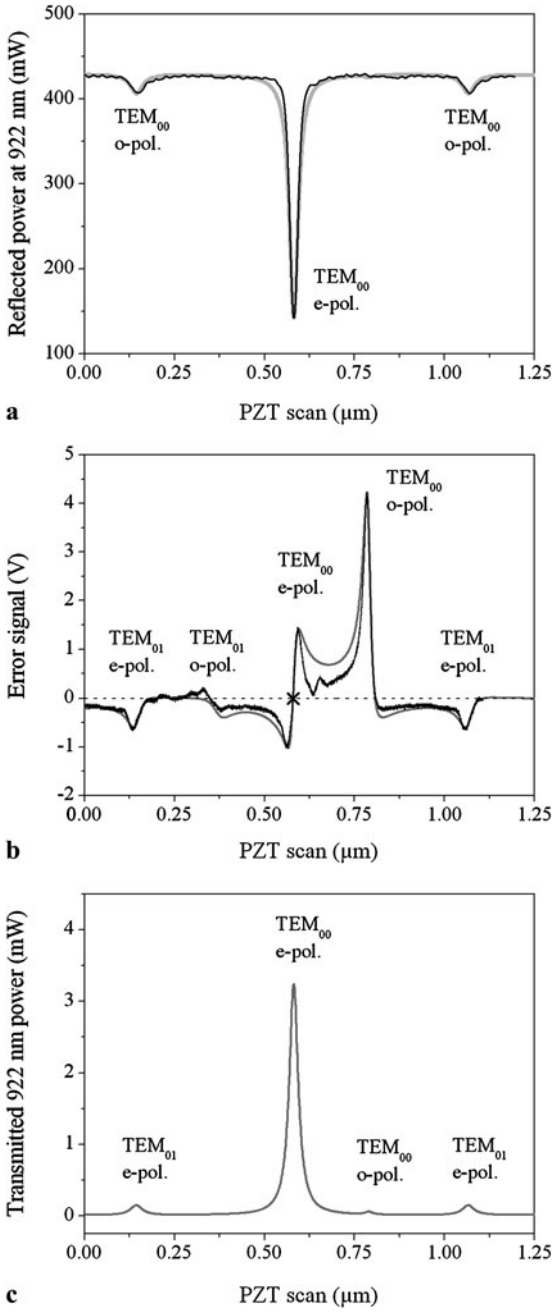

Fig. 6 (**a**) Pump power reflected from the input mirror of the build-up cavity as a function of cavity length scan. (**b**) The corresponding HC error signal obtained in the transmission-mode. The lock-point (*zero-crossing point*) is denoted by a cross. (**c**) The corresponding power spectrum of the light transmitted through the cavity to the HC detector. *Black curves* are measured signals and *gray curves* are simulations

peaks of the *e*-polarized wave, and hence the respective error signal features, appear slightly broadened in the simulated spectra. This is a result of neglecting the dependence of nonlinear loss Γ on cavity detuning in the simulation (see Sect. 2). Furthermore, the real error signal spectrum reveals weak peaks of TEM_{11} transverse modes that were not included in the simulation.

Mode-matching coefficients for the *o*-polarized wave were observed to be sensitive to changes in the input beam alignment and significantly different compared to those of the *e*-polarized wave. While the cavity alignment and mode-matching are optimized for the TEM_{00} mode of the *e*-polarized wave, the *o*-polarized wave experiences significant excitation of several higher order transverse modes. When the alignment was optimized for the *o*-polarized wave, its mode matching became much better and that of the *e*-polarized wave got worse. This behavior was not studied in detail but it is likely that the small tilt of the PPKT relative to the optical axis, as discussed above, makes the two polarizations have different alignments for which their coupling into the cavity is optimized. Because we couple only a small amount (0.5–2%) of the total pump power into the *o*-polarization, the excitation of a large number of relatively strong *o*-polarized side modes does not cause a problem. Usually, only the TEM_{01} and sometimes TEM_{11} modes of the *o*-polarized wave have sufficient intensity to show up in the error signal; see Fig. 6b.

The lock point, which is the zero-cross point of the error signal (Fig. 6b), can be adjusted for maximum blue output power either by rotating the quarter wave plate or by adjusting the relative gains of the two photodetector signals of the HC detector assembly. Fine adjustment is done using the error signal offset potentiometer. Proper adjustment of the lock point is important not only for maximizing the blue output power but also for ensuring good power stability. If the ECDL frequency is not locked at the exact center of a cavity resonance, any uncompensated frequency fluctuation of the ECDL or build-up cavity relative to each other is converted into an amplitude fluctuation. As an example, if the lock point is shifted from the resonance center by 2 MHz, laser frequency noise (relative to the build-up cavity) of as small as 1 MHz peak-to-peak converts to 2% peak-to-peak power noise at blue. This was calculated based on the measured hot-cavity linewidth of 26 MHz ($F = 30$, $FSR = 780$ MHz) of our build-up cavity, taking into account that any change in the intracavity 922 nm power quadratically converts into power fluctuations of the 461 nm light.

With the lock-point properly adjusted, we achieve high stability of the blue output power, with RMS power fluctuation of well below 1% as demonstrated in Fig. 7. For long time periods of several hours or more, we often see larger power fluctuations of up to several percent peak-to-peak, owing to drifting of the cavity lock point either due to crystal/cavity temperature drift or servo electronics drift. Small manual adjustment of the lock point is then needed to maintain the high power stability.

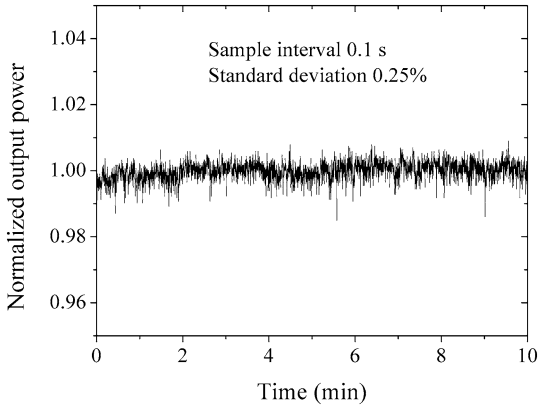

Fig. 7 Measured stability of the blue output power through mirror M2 (see Fig. 4). The average output power is 185 mW

Frequency of the output beam can be fine tuned without mode hops using the PZT actuator attached to one of the cavity mirrors. As the ECDL frequency is locked to the cavity frequency, it follows the tuning until the ECDL makes a mode hop. Fine tuning range at 922 nm is about 4–4.5 GHz, which is limited by the mode-hop-free tuning range of the ECDL. At the doubled frequency 2ω, this converts to a tuning range of 8–9 GHz. After setting the frequency to a given value, passive frequency instability at 461 nm is typically better than 500 MHz over several hours. This has been measured by optogalvanic spectroscopy with a Sr hollow cathode lamp. The blue output beam of the frequency doubler was passed through the Sr hollow cathode lamp and its frequency was monitored against the Sr absorption peak. The frequency scale was obtained by calibrating the absorption peak linewidth with a wavelength meter.

5 Conclusions

We have reported a cw cavity-enhanced optical frequency doubler based on a modified version of the Hänsch–Couillaud technique for locking the pump laser to the build-up cavity of the frequency doubler. Similarly to conventional Hänsch–Couillaud locking, the error signal for locking is obtained by using polarization spectroscopy to measure the pump laser frequency deviation relative to a resonance peak of the build-up cavity. While in the conventional approach this measurement is done using the light reflected by the cavity, we have used cavity transmission. The transmitted beam is spectrally and spatially filtered by the cavity, which ensures a clean error signal despite possible high-order transverse modes in the pump beam.

A detailed analysis and comparison of the reflection- and transmission-mode Hänsch–Couillaud techniques in the

context of cavity-enhanced frequency doubling has been presented, together with an experimental demonstration of the transmission-mode method. We have applied the method to generation of cw single-frequency light at 461 nm. The frequency doubler is pumped by a MOPA, which consists of a widely tunable external-cavity diode laser and a tapered amplifier. High blue output power of 200 mW, excellent power stability of better than 1%, and mode-hop-free frequency tuning range of >8 GHz have been achieved. Moreover, we have described a simple method for optimizing the locking error signal spectrum: a rotatable wave plate inside the cavity can be used to adjust the cavity birefringence in order to avoid spectral overlapping of orthogonal polarization components of the laser light circulating in the cavity. In this manner, a clean dispersion-like error signal around the desired cavity transmission peak can be obtained.

Acknowledgements The authors would like to thank R. Pelletier for technological support in the development of electronics needed in the experiment. M. Vainio thanks the Academy of Finland for financial support (Grants Nos. 125111 and 132881).

References

1. R. Le Targat, J.-J. Zondy, P. Lemonde, Opt. Commun. **247**, 471 (2005)
2. N. Poli, G. Ferrari, M. Prevedelli, F. Sorrentino, R.E. Drullinger, G.M. Tino, Spectrochim. Acta, Part A, Mol. Biomol. Spectrosc. **63**, 981 (2006)
3. X. Xu, T.H. Loftus, J.L. Hall, A. Gallagher, J. Ye, J. Opt. Soc. Am. B **20**, 968 (2003)
4. C.W. Oates, F. Bondu, R.W. Fox, L. Hollberg, Eur. Phys. J. D **7**, 449 (1999)
5. F. Torabi-Goudarzi, E. Riis, Opt. Commun. **227**, 389 (2003)
6. M. Bode, I. Freitag, A. Tünnermann, H. Welling, Opt. Lett. **22**, 1220 (1997)
7. A.D. White, IEEE J. Quantum Electron. **QE-l**, 349 (1965)
8. R.W.P. Drever, J.L. Hall, F.V. Kowalski, J. Hough, G.M. Ford, A.J. Munley, H. Ward, Appl. Phys. B, Photophys. Laser Chem. B **31**, 97 (1983)
9. T.W. Hänsch, B. Couillaud, Opt. Commun. **35**, 441 (1980)
10. A. Hemmerich, D.H. McIntire, C. Zimmermann, T.W. Hänsch, Opt. Lett. **15**, 372 (1990)
11. U. Sterr, B. Lipphardt, A. Wolf, H.R. Telle, IEEE Trans. Instrum. Meas. **48**, 574 (1999)
12. N. Nemitz, Setup of a stable high-resolution laser system. Diploma thesis, University of Stuttgart, 2004
13. W.J. Kozlovsky, C.D. Nabors, R.L. Byer, J. Quantum Electron. **24**, 913 (1988)
14. M. Born, E. Wolf, *Principles of Optics* (Pergamon, Elmsford, 1999), Chap. 7.6.1
15. O. Svelto, *Principles of Lasers* (Springer, Berlin, 2010)
16. J.M. Boon-Engering, W.E. van der Veer, E.A.J.M. Bente, W. Hogervorst, Opt. Commun. **140**, 285 (1997)
17. C.J. Hawthorn, K.P. Weber, R.E. Scholten, Rev. Sci. Instrum. **72**, 4477 (2001)
18. G. Boyd, D. Kleinman, J. Appl. Phys. **39**, 3597 (1968)
19. C.E. Wieman, S.L. Gilbert, Opt. Lett. **7**, 480 (1982)
20. D. Schnier, A.A. Madej, Opt. Commun. **105**, 388 (1994)
21. D.A. Shaddock, M.B. Gray, D.E. McClelland, Opt. Lett. **24**, 1499 (1999)